HHS Public Access

Author manuscript

Curr Opin Neurobiol. Author manuscript; available in PMC 2019 June 01.

Published in final edited form as:

Curr Opin Neurobiol. 2018 June ; 50: 250–260. doi:10.1016/j.conb.2018.04.026.

Magnetic Resonance Imaging technology – bridging the gap between noninvasive human imaging and optical microscopy

Jonathan R. Polimeni[1,2] and **Lawrence L. Wald**[1,2]

[1]Athinoula A. Martinos Center for Biomedical Imaging, Dept. of Radiology, Harvard Medical School, Massachusetts General Hospital, Charlestown, MA, USA

[2]Harvard-Massachusetts Institute of Technology Division of Health Sciences and Technology, Cambridge, MA, USA

Abstract

Technological advances in Magnetic Resonance Imaging (MRI) have provided substantial gains in the sensitivity and specificity of functional neuroimaging. Mounting evidence demonstrates that the hemodynamic changes utilized in functional MRI can be far more spatially and thus neuronally specific than previously believed. This has motivated a push toward novel, high-resolution MR imaging strategies that can match this biological resolution limit while recording from the entire human brain. While sensitivity increases are a necessary component, new MR encoding technologies are required to convert improved sensitivity into higher resolution. These new sampling strategies improve image acquisition efficiency and enable increased image encoding in the time-frame needed to follow hemodynamic changes associated with brain activation.

Keywords

functional magnetic resonance imaging; human neuroimaging; ultra-high field MRI; MRI instrumentation & technology; high-resolution fMRI; parallel imaging

INTRODUCTION

The traditional strength of functional MRI (fMRI) has been its ability to non-invasively image hemodynamic responses including changes in blood flow, volume and oxygenation associated with brain function over large regions, including the entire human brain. Although MRI technology has focused on methods allowing the study of smaller and smaller structures while retaining its whole-brain coverage, invasive methods using multi-photon and light-sheet fluorescence microscopy have an inherent ability to image down to the neuron scale but have expanded on the opposite front—moving from small fields of view to larger territories, including entire brain regions [1–5] (see Fig. 1).

Correspondence should be directed to: Jon Polimeni, Ph.D., MGH Athinoula A. Martinos Center for Biomedical Imaging, Bldg 149 13th St Rm 2301, Charlestown MA, 02129 USA., Tel: +1 617 724 4546, Fax: +1 617 726 7422, jonp@nmr.mgh.harvard.edu.

As these two technologies meet, they will eliminate a gap in our *in vivo* imaging capability, providing an unprecedented opportunity to translate insights from small animal studies directly to human studies and also greatly inform the mechanisms underpinning fMRI. For example, functional connectivity derived from resting-state fMRI has withstood many indirect validations, but its fundamental tenant—that correlations in the hemodynamic signals reflect correlated neuronal firing patterns—was only recently directly demonstrated using wide-field microscopy experiments [2]. This bridging of the scales is a powerful motivator to extend human neuroimaging with MRI toward studies of smaller-scale functional circuitry. The goal of this review is to examine recent MRI advances in MRI system hardware, data acquisition, and image reconstruction strategies that are being pursued to achieve this goal.

The push toward higher spatio-temporal resolution MRI is not new [6]; but it has not been straightforward to "turn up the magnification" to enhance the resolution of an MRI experiment. It is not only hardware limitations (i.e., a lack of bigger magnets) standing in the way, but also performance restrictions. Improved sampling strategies are needed to acquire the additional information at the highest spatio-temporal resolution allowed by hemodynamics. Increasing performance also requires attention to safe operation of the scanner for human subjects. In practice, these goals require coordinated improvements in all aspects of the MRI acquisition.

Current state-of-the-practice and potential biological limits of the spatial-temporal resolution of hemodynamics-based fMRI

Current practice (2–4 mm resolution in 3 Tesla magnets and 1–2 mm in 7 Tesla magnets) is firmly limited by MRI technology rather than any biological limit. In this review, we consider only *isotropic* spatial encoding strategies; in our view, isotropic voxels are needed to provide spatially-unbiased sampling over large brain regions. Invasive animal-model studies suggest that blood flow regulation is more precise both spatially [7,8] and temporally [9,10] than the 2–5 mm that have traditionally been considered the "hemodynamic limit" [11]. Hemodynamic control has been shown to be regulated at the 200 μm scale in the rodent olfactory bulb [12,13], and, in less-specialized cortex, blood flow regulation has been seen at the capillary or precapillary levels [14,15]. Importantly, these observations place the unit of regulatory control at a smaller scale than even current high-resolution fMRI studies, although an observation in one structure does not necessarily generalize to all brain regions. Nonetheless, these studies suggest that if improved instrumentation can be built, it will enable mapping of finer levels of neural activation.

Although the Blood-Oxygenation-Level-Dependent (BOLD) contrast is by far the most robust and commonly used signal used in fMRI, alternative techniques may provide enhanced neuronal specificity. Notably, fMRI based on changes in cerebral blood volume may increase sensitivity to the capillary bed, improving localization of neuronal activity [16,17]. This technology has been recently extended to human imaging [18–22]. New techniques aimed at non-hemodynamic signals such as the detection of cell swelling [23–25] or neuronal current oscillations [26–29] also hold promise. However, these new techniques

require further investigation, are limited by low sensitivity, and face the same image resolution and coverage challenges as conventional fMRI.

INCREASING SENSITIVITY: BIG MAGNETS AND MASSIVELY-PARALLEL DETECTORS

The sensitivity of the detected MR signal decreases as the voxel volume; thus, a 3-mm cubic voxel has 27-fold higher signal level than a 1-mm cubic voxel. This rapid loss of signal amplitude immediately motivates improvements in the key technologies that define signal sensitivity: the static magnetic field (B_0) and the detection array coil.

Ultra-high magnetic field strengths

Not only does image signal-to-noise ratio (SNR) increase supra-linearly with magnetic field strength [30], but in the case of the standard fMRI signal—the BOLD contrast—the image contrast between the active and baseline states also increases, providing a substantial boost in contrast-to-noise ratio at high fields. Furthermore, the BOLD fMRI signal becomes more specific to the smallest intracortical blood vessels and capillaries with increasing field strength [31]. Thus, at high fields, BOLD reflects signal changes in the vascular compartment where the coupling between neuronal activity and the hemodynamic signals is tightest, therefore the neuronal specificity of fMRI is enhanced at high fields. These are the key motivations for the recent push for *ultra-high-field* MRI—defined as MRI at fields above 7 Tesla—for functional neuroimaging.

Increasing the magnetic field is the most direct means to increase sensitivity and specificity, but with higher fields come many challenges for imaging, including: artifacts and distortions associated with magnetic susceptibility and transmission wavelength effects in the human head, safety limitations due to radiofrequency (RF) power deposition, and amplification of physiological noise. Fortunately, concerted engineering efforts have addressed many of these issues, several of which are summarized below and in recent review articles [32]. An example of the improvements in image quality afforded by these efforts is presented in Fig. 2. Because of the success of the current generation of 7 Tesla and 9.4 Tesla human MRI scanners, recent efforts have evaluated the safety and engineering challenges of even higher magnetic field strengths (10.5 Tesla and 11.7 Tesla), and conclude that fields up to 20 Tesla would be feasible and would provide even further gains in sensitivity and specificity, opening the door to new applications [33–35].

RF coil arrays

Perhaps the single most significant engineering solution to the challenges of ultra-high-field MRI is the advent of RF receive coil arrays comprised of many detector channels operating in parallel, which arrived just after the introduction of 7 Tesla human scanners. There are two advantages to using a large number of smaller detectors to cover the head: SNR is increased (especially in the cortex); and parallel imaging performance improves, facilitating fast image encoding. Combining these into a single metric, we consider *accelerated SNR*, or the SNR of the accelerated, undersampled acquisitions used in parallel imaging, which has been shown to increase rapidly with higher-channel-count arrays [36]. The acceleration of

the fMRI acquisition reduces artifacts such as image blurring and distortion [37–39]. This has inspired a trend towards larger brain arrays [40–42] and also dense arrays tailored to specific brain regions, such as 32-channel coils centered on the visual cortex or motor cortex [43–45].

NEW SAMPLING STRATEGIES TO OVERCOME ENCODING LIMITS

Although parallel imaging techniques have allowed the exploitation of data undersampling to pack in more image encoding per unit time, new image reconstruction strategies emphasize the role of the undersampling pattern design to reduce inefficiencies or redundancies in the encoding. These ideas exploit older concepts about the efficiency of 3D image encoding, and very benign forms of prior knowledge (such as “the head is round-ish”) as well as more strict assumptions about image compressibility. The result is more encoding per unit time—a critical goal for bringing instrumental resolution down to the biological limits. Several of these undersampling strategies are highlighted in Fig. 3 and explained further below.

Controlled Aliasing in Parallel Imaging (*CAIPI*) *and* Simultaneous Multi-Slice *Imaging*

Although early parallel imaging methods provided huge benefits to fMRI, Controlled Aliasing In Parallel Imaging (“CAIPI”), and the Simultaneous Multi-Slice methods it has enabled, are probably the most impactful second-generation parallel imaging methods. The goal of parallel imaging reconstruction is to remove aliasing incurred by undersampling the acquisition through leveraging the partially redundant information afforded by the coil array [46,47]. The pattern of the aliasing, however, is determined by the sampling pattern. In the CAIPI approach [48], the overall degree of image aliasing is lowered by forcing the aliasing replicates to fall in signal-void regions e.g. outside of the head, yielding a simpler reconstruction with fewer residual artifacts and less noise amplification. This concept has provided tremendous gains in anatomical imaging, especially in applications using 3D image encoding [49]. The sampling strategy can also be changed dynamically when combining data across multiple repeated acquisitions [50] or different image contrasts [51] to further suppress artifacts enabling even faster acquisitions.

The concept of CAIPI can be extended to the readout direction by utilizing “zig-zag” [52], “bunched phase encoding” [53], or “corkscrew”/“wave” [54–56] k-space sampling trajectories. This further spreads out aliasing in multiple directions to provide increased imaging performance, providing over an order of magnitude speed-up compared to conventional acquisitions [57,58].

Simultaneous Multi-Slice imaging [59,60] is a parallel imaging technique that can also benefit from CAIPI [48,61]. Simultaneous Multi-Slice imaging was recently extended to echo-planar imaging (EPI), the “snapshot” imaging method most commonly used for fMRI, and has already provided major benefits to fMRI [62–64]. The addition of CAIPI to Simultaneous Multi-Slice EPI was attempted early on [60] and was ultimately achieved by a balanced z-gradient blip train to impose the CAIPI slice shifts, providing dramatic improvements in image quality and SNR [62]. This has enabled acceleration factors of up to 10 simultaneous slices with conventional coil arrays [65]. Acceleration of encoding in the is

an enabling technology for high isotropic resolution, whole-brain imaging. Without it, acquiring all the slices during the timescale afforded by hemodynamic changes (~3 s) is not possible.

Compressed Sensing

Compressed Sensing is a conceptually-related technique in which the sampling pattern is designed to be pseudo-random or irregular to impose unstructured aliasing (i.e., mimicking noise, see Fig. 3B). The pseudo-random sampling is combined with a prior assumption that the image can be represented in some transform domain with a sparse set of coefficients (i.e. the image information is highly compressible) [66]. Not only can Compressed Sensing techniques provide large gains in encoding efficiency for classes of images that can be sparsely represented in a transform domain (e.g., the wavelet domain or the Fourier domain), but their application to MRI merged the powerful concepts of tailored sampling and model-based reconstruction.

Magnetic Resonance Fingerprinting

Magnetic Resonance Fingerprinting is a recent concept that builds off of the insights of CAIPI, Compressed Sensing, and model-based reconstruction, with a goal of providing quantitative maps of tissue relaxation properties as potential imaging biomarkers [67]. In Magnetic Resonance Fingerprinting, the various pulse sequence parameters that control image contrast are varied in time pseudo-randomly. A model of the time-evolution of the signal as a function of the tissue properties of interest (e.g., longitudinal magnetization relaxation time T_1, irreversible transverse relaxation time T_2, apparent diffusion coefficient) and nuisance factors (e.g., local magnetic field offset ΔB_0, transmit field B_1^-, coil sensitivity B_1^+) and generates a “fingerprint”. A dictionary of pre-computed fingerprints is compared against the measured signal evolution of each voxel using fast pattern matching to find the tissue parameter values [67]. As with Compressed Sensing, Magnetic Resonance Fingerprinting exploits the incoherence of aliasing artifacts imparted by the pseudo-random acquisition—although any given image may have artifacts, the artifact pattern varies over time such that the final parameter maps have lower artifact levels. Although promising for clinical MRI, Magnetic Resonance Fingerprinting has not yet found a role in fMRI studies.

Image reconstruction with Machine Learning

Although the application of Machine Learning to MRI reconstruction is extremely new, recent demonstrations have shown that supervised Machine Learning techniques, such as the convolutional neural networks (which form the basis of many Deep Learning algorithms), can be adequately trained on example data and generalize sufficiently to reconstruct data not in the training set [68–71]. The key applications likely to benefit most or to be enabled by Machine Learning remain to be seen, but early indications suggest that Machine Learning may find a prominent role in MR image reconstruction, the design of efficient acquisition schemes, or in removing complex artifacts such as those caused by subject motion.

REDUCING ENCODING BURDEN

Although faster image encoding and tailored sampling schemes can help achieve higher spatiotemporal resolution while avoiding image artifacts and blurring, there are several technologies that can be applied to reducing the encoding burden, for example by either decreasing the *required* number of encoding steps by reducing the spatial extent of the image, or by homogenizing the magnetic field.

RF transmission techniques for reduced encoding

As discussed above, achieving high spatial resolution requires many encoding steps. Because MRI uses Fourier encoding, the full extent of the anatomy intersecting a slice must be encoded, which, for those cases where only a small brain region is under investigation, prolongs image encoding, reduces efficiency, and causes increased image blurring [32]. One common strategy to eliminate signal from tissue outside of the region of interest, and thereby reduce the required number of encoding steps, is to utilize “zoomed” imaging, which either selectively excites only the tissue within the region of interest, or selectively suppresses tissue outside of the region of interest [32]. This can dramatically shorten the encoding time to allow for higher resolution [72,73]. Emerging parallel transmission techniques can provide for sharper definition of these zoomed regions to reduce artifacts associated with imperfect selective excitation or signal suppression [74–76]. The additional degrees of freedom in parallel transmission can also be used to cancel the electric fields and thereby reduce Specific Absorption Rate and tissue heating associated with these RF pulses [77,78].

B_0 shimming

B_0 inhomogeneity places additional burden on image encoding by increasing the need for parallel imaging acceleration to reduce distortion and blurring. The field inhomogeneity arises from complex patterns of fields as tissue magnetize in the large applied magnetic field, especially those around air-tissue interfaces. The “shimming” process attempts to eliminate these field nonuniformities and homogenize the B_0 field. Although conventional B_0 shimming using spherical harmonic shim coils built into the scanner has been sufficient in the past, we now see the need for local arrays of shim coils placed close to the head. These provide additional degrees of freedom to efficiently homogenize the field [79,80]. A new “AC/DC” design has emerged that can integrate the shimming elements (“DC”) with the RF detector coils (“AC”) such that both share the same conductor and do not compete for precious real estate around the head [81,82]. Advances in high-field shimming and field control have recently been reviewed [83].

Magnetic field monitoring, corrections, and feedback

Image encoding requires accurate control of the magnetic fields within the head during readout, and any uncompensated field gradients—either from lack of full calibration of the gradient system to dynamic gradients created by subject respiration—can cause artifacts and modulations of the image time-series. Magnetic field sensing probes have been recently introduced to measure and correct for these imperfections [84,85]. These probes measure the field at a single point in space concurrently with the imaging, and arrays of probes can be

used as a “field camera” for scanner calibration [86,87] or acquisition-specific corrections [88]. They can also be positioned around the subject during scanning to dynamically monitor the fields. This information can be used either to feed these signals back into the system for real-time correction [85] or to remove artifacts during the image reconstruction [89]. Recent demonstrations have shown that probes embedded within the patient table can measure the field changes induced by the subject’s cardiac cycle [90,91], which can be used to either prospectively synchronize the measurement to the heart rate to remove pulsatile blood flow or related motion artifacts, or retrospectively regress out physiological noise from the image data.

SPECIALIZED AND MULTI-MODAL MRI SCANNERS FOR NEUROSCIENCE

Since neuroscience (as opposed to clinical imaging) forms the sole use of a growing fleet of MRI scanners, there has been a recent trend towards specialized MRI scanners with hardware tailored to functional imaging for neuroscience studies.

Gradient coils for functional MRI: increasing slew rate

The performance of gradient coils was previously limited by engineering concerns, such as achieving a spatially-linear gradient field, removal of heat from the coil, and the efficiency and power requirements of the coil. These issues are now largely resolved, and the main limiting factor on whole-body gradient performance is the bioeffects of rapidly switching, large magnetic fields on the human body. Peripheral Nerve Stimulation (PNS) can be induced if the product of the gradient switching rate and strength generate electric fields large enough to trigger nerve firing, which manifests as discomfort or pain. PNS is therefore strictly regulated in MRI. A smaller head gradient coil that covers only the subject’s head and neck eliminates the induction of large current paths in the chest and back which are prone to stimulation and thus offers a simple strategy for reducing PNS in brain imaging. Although head gradient coils with fast switching speed and strong gradients have been in use for some time [92], the new sensitivity afforded by higher field strengths and the increasing need for faster encoding has created a renaissance in head gradient coil use [93–95] for fMRI.

Although gradient coil manufacturers have heuristics to design coils that avoid PNS, ultimately the ability of a coil to prevent PNS is only known once the coil is constructed and operated. Recent work has shown that numerical body models with explicit human nerve anatomy combined with nerve dynamics models can closely predict PNS levels measured in volunteers [96]. This approach has the potential to accelerate testing and save cost, by providing PNS predictions that can be fed back into the design process to potentially improve gradient coil performance applicable to human imaging.

Similar to RF coil arrays, “matrix gradient coils” provide additional spatial degrees of freedom for encoding, potentially allowing increased efficiency or PNS control [97,98]. Often these gradient coils relax the linearity constraint of the gradient field, introducing non-bijective, non-Fourier encoding [99,100]. Early attempts to utilize these novel encoding schemes are being explored in the PArallel imaging Technique using LOCalized gradients or “PatLoc” framework [101] and in O-space imaging [102].

Gradient coils for diffusion MRI: increasing gradient strength

For diffusion imaging, gradient coils capable of producing gradient fields with high amplitudes provide high degrees of diffusion encoding in less time. This translates into a large boost in signal level by reducing signal decay from T_2 relaxation. Thus diffusion has been a primary motivation for recent dedicated gradient coils with large maximum gradient amplitudes [103–107]. For example, the “Connectom” gradient coil (designed for the *Human Connectome Project*) utilized a segmented design with four power amplifiers per physical axis (so 12 total) to overcome efficiency limits [103]. Unlike high-resolution EPI readouts, diffusion encoding has relatively low slew-rate requirements, and therefore avoids PNS issues.

Combined modalities: PET-fMRI, EEG-fMRI, TMS-fMRI, and potential of MR-tFUS

Because the various human neuroimaging and neuromodulation modalities can access different aspects of brain function, ongoing work seeks to merge their unique capabilities to extract new information about human brain function and organization. Continued development of instrumentation and technologies for integrating fMRI with Positron Emission Tomography (PET) [108–112], Electro-Encephalography (EEG) [113–116], and Transcranial Magnetic Stimulation (TMS) [117,118] has addressed many of the challenges faced when introducing additional equipment into the MRI environment. Recent work combining MRI with ultrasound may pave the way to integration with transcranial Focused Ultrasound (tFUS) [119], and progress using ultrasound to stimulate neuron populations [120,121] may in the future provide key insights into brain function and neurovascular coupling once the mechanisms of neuronal stimulation are better understood [122,123]. These multi-modal approaches can be used to synergistically merge the hemodynamic signals measured in fMRI with complementary metabolic and electrical signals, and image whole-brain responses to targeted neuromodulation, to both enhance neuronal specificity and map large-scale brain circuitry.

CONCLUSIONS

Several themes emerge from reviewing recent trends and advancements in MRI technologies for neuroscience. MRI technology has been effective at utilizing increasing degrees of freedom both in the sensors (RF detectors, motion cameras, field probes) and effectors (RF transmitters, B_0 shim arrays, gradient arrays). There is also movement toward dedicated MRI scanners that excel at a desired form of imaging such as fMRI or MR diffusion imaging. New insights into increased encoding efficiency in image sampling have provided improved encoding and image reconstruction algorithms. Overall, these techniques have improved the sensitivity, resolution, and functional contrast to advance toward improved whole-brain, high-resolution non-invasive measurement of brain function in humans which maximally leverages the neuronal specificity of the fMRI signals.

Acknowledgments

We gratefully acknowledge Drs. Bastien Guérin, Kawin Setsompop, and Thomas Witzel for helpful comments, and Dr. Berkin Bilgic for help with the wave-CAIPI sampling simulation. This work was supported in part was supported in part by the NIH NIBIB (grants P41-EB015896, R01-EB023281, and R01-EB019437), by the NEI

(R01-EY026881), by the *BRAIN Initiative* (NIMH grants R01-MH111419, R01-MH111438, R24-MH106053, and R24-MH106096 and NIBIB grants U01-EB025162 and U01-EB025121), and by the MGH/HST Athinoula A. Martinos Center for Biomedical Imaging.

REFERENCES AND RECOMMENDED READING

• of special interest

•• of outstanding interest

1. Kim TH, Zhang Y, Lecoq J, Jung JC, Li J, Zeng H, Niell CM, Schnitzer MJ. Long-term optical access to an estimated one million neurons in the live mouse cortex. Cell Rep. 2016; 17:3385–3394. [PubMed: 28009304]

2••. Ma Y, Shaik MA, Kozberg MG, Kim SH, Portes JP, Timerman D, Hillman EMC. Resting-state hemodynamics are spatiotemporally coupled to synchronized and symmetric neural activity in excitatory neurons. Proc Natl Acad Sci U S A. 2016; 113:E8463–E8471. This study used wide-field optical imaging to measure both calcium dynamics of neurons (GCaMP) and the associated hemodynamics (intrinsic signals) to investigate the relationship between spontaneous neural activity and the hemodynamic fluctuations that form the basis of fMRI. They find that resting-state hemodynamics are coupled to underlying patterns of neural activity, and that both the hemodynamics and neural activity exhibit wide-range and mirror-symmetric spatial patterns of correlations across the two cerebral hemispheres. [PubMed: 27974609]

3. Yang W, Miller JK, Carrillo-Reid L, Pnevmatikakis E, Paninski L, Yuste R, Peterka DS. Simultaneous multi-plane imaging of neural circuits. Neuron. 2016; 89:269–284. [PubMed: 26774159]

4. Sofroniew NJ, Flickinger D, King J, Svoboda K. A large field of view two-photon mesoscope with subcellular resolution for in vivo imaging. Elife. 2016; 5:e14472. [PubMed: 27300105]

5. Tsai PS, Mateo C, Field JJ, Schaffer CB, Anderson ME, Kleinfeld D. Ultra-large field-of-view two-photon microscopy. Opt Express. 2015; 23:13833. [PubMed: 26072755]

6. Yacoub E, Wald LL. Pushing the spatio-temporal limits of MRI and fMRI. Neuroimage. 2018; 164:1–3. [PubMed: 29254519]

7. Hamilton NB, Attwell D, Hall CN. Pericyte-mediated regulation of capillary diameter: a component of neurovascular coupling in health and disease. Front Neuroenergetics. 2010; 2:1–14. [PubMed: 20162100]

8•. Longden TA, Dabertrand F, Koide M, Gonzales AL, Tykocki NR, Brayden JE, Hill-Eubanks D, Nelson MT. Capillary K+-sensing initiates retrograde hyperpolarization to increase local cerebral blood flow. Nat Neurosci. 2017; 20:717–726. This article identifies a potentially new pathway of neurovascular coupling in which capillary endothelial cells sense extracellular K+, a byproduct of neural activity, which triggers a “rapidly propagating retrograde hyperpolarization that causes upstream arteriolar dilation”. While similar propagation of signals along microvessels has been previously observed and reported, the authors here suggest that capillaries may form a “sensory web” that can rapidly respond to local electrical neural activity. [PubMed: 28319610]

9•. Nizar K, Uhlirova H, Tian P, Saisan PA, Cheng Q, Reznichenko L, Weldy KL, Steed TC, Sridhar VB, Macdonald CL, et al. In vivo stimulus-induced vasodilation occurs without IP3 receptor activation and may precede astrocytic calcium increase. J Neurosci. 2013; 33:8411–8422. Using two-photon imaging of individual vessel diameter changes and fluorescence imaging of calcium dynamics in neighboring astrocytes, these authors demonstrate that the vascular response to neuronal activity can precede the astrocytic calcium by nearly 3 s. Not only does this suggest that astrocyte dynamics are too slow to initiate vasodilation in this case, questioning the role of astrocytes in neurovascular coupling, but it also demonstrates how rapid the local vascular response to neuronal activity can be. [PubMed: 23658179]

10. Tian P, Teng IC, May LD, Kurz R, Lu K, Scadeng M, Hillman EMC, De Crespigny AJ, D’Arceuil HE, Mandeville JB, et al. Cortical depth-specific microvascular dilation underlies laminar differences in blood oxygenation level-dependent functional MRI signal. Proc Natl Acad Sci U S A. 2010; 107:15246–51. [PubMed: 20696904]

11. Logothetis NK, Wandell BA. Interpreting the BOLD signal. Annu Rev Physiol. 2004; 66:735–69. [PubMed: 14977420]
12. Poplawsky AJ, Fukuda M, Murphy M, Kim S-G. Layer-specific fMRI responses to excitatory and inhibitory neuronal activities in the olfactory bulb. J Neurosci. 2015; 35:15263–75. [PubMed: 26586815]
13. Poplawsky AJ, Fukuda M, Kang B, Kim JH, Suh M, Kim S-G. Dominance of layer-specific microvessel dilation in contrast-enhanced high-resolution fMRI: Comparison between hemodynamic spread and vascular architecture with CLARITY. Neuroimage. 2018; doi: 10.1016/j.neuroimage.2017.08.046
14•. Hall CN, Reynell C, Gesslein B, Hamilton NB, Mishra A, Sutherland BA, O'Farrell FM, Buchan AM, Lauritzen M, Attwell D. Capillary pericytes regulate cerebral blood flow in health and disease. Nature. 2014; 508:55–60. This study follows up from prior work from this group where they demonstrated the potential for pericytes to regulate capillary diameter through a series of measurements made in excised tissue. In this new work they demonstrate that pericytes dilate capillaries in vivo, and that this dilation precedes upstream arteriole dilation. [PubMed: 24670647]
15•. Hill RA, Tong L, Yuan P, Murikinati S, Gupta S, Grutzendler J. Regional blood flow in the normal and ischemic brain is controlled by arteriolar smooth muscle cell contractility and not by capillary pericytes. Neuron. 2015; 87:95–110. In contrast to the Hall et al. study, this article suggests that the contractile elements that cause microvascular dilation may not be pericytes but rather may be smooth muscle cells, and that the observed dilation may be occuring at pre-capillary arterioles. Nevertheless, this study indicates that cerebral blood flow is regulated in a much finer spatial and temporal scale than previously believed, and identifies one such mechanism supporting this local blood flow control. [PubMed: 26119027]
16. Mandeville JB, Marota JJ. Vascular filters of functional MRI: spatial localization using BOLD and CBV contrast. Magn Reson Med. 1999; 42:591–8. [PubMed: 10467305]
17. Zhao F, Wang P, Hendrich K, Uğurbil K, Kim S. Cortical layer-dependent BOLD and CBV responses measured by spin-echo and gradient-echo fMRI: insights into hemodynamic regulation. Neuroimage. 2006; 30:1149–60. [PubMed: 16414284]
18. Qiu D, Zaharchuk G, Christen T, Ni WW, Moseley ME. Contrast-enhanced functional blood volume imaging (CE-fBVI): enhanced sensitivity for brain activation in humans using the ultrasmall superparamagnetic iron oxide agent ferumoxytol. Neuroimage. 2012; 62:1726–31. [PubMed: 22584230]
19. D'Arceuil H, Coimbra A, Triano P, Dougherty M, Mello J, Moseley M, Glover G, Lansberg M, Blankenberg F. Ferumoxytol enhanced resting state fMRI and relative cerebral blood volume mapping in normal human brain. Neuroimage. 2013; 83:200–9. [PubMed: 23831413]
20. Huber L, Ivanov D, Krieger SN, Streicher MN, Mildner T, Poser BA, Möller HE, Turner R. Slab-selective, BOLD-corrected VASO at 7 Tesla provides measures of cerebral blood volume reactivity with high signal-to-noise ratio. Magn Reson Med. 2014; 72:137–48. [PubMed: 23963641]
21. Huber L, Handwerker DA, Jangraw DC, Chen G, Hall A, Stüber C, Gonzalez-Castillo J, Ivanov D, Marrett S, Guidi M, et al. High-resolution CBV-fMRI allows mapping of laminar activity and connectivity of cortical input and output in human M1. Neuron. 2017; 96:1253–1263.e7. [PubMed: 29224727]
22. Lu H, Golay X, Pekar JJ, Van Zijl PCM. Functional magnetic resonance imaging based on changes in vascular space occupancy. Magn Reson Med. 2003; 50:263–74. [PubMed: 12876702]
23. Bai R, Stewart CV, Plenz D, Basser PJ. Assessing the sensitivity of diffusion MRI to detect neuronal activity directly. Proc Natl Acad Sci U S A. 2016; 113:E1728–37. [PubMed: 26941239]
24. Tsurugizawa T, Ciobanu L, Le Bihan D. Water diffusion in brain cortex closely tracks underlying neuronal activity. Proc Natl Acad Sci U S A. 2013; 110:11636–11641. [PubMed: 23801756]
25. Williams RJ, Reutens DC, Hocking J. Influence of BOLD contributions to diffusion fMRI activation of the visual cortex. Front Neurosci. 2016; 10:279. [PubMed: 27445654]
26. Witzel T, Lin F-H, Rosen BR, Wald LL. Stimulus-induced Rotary Saturation (SIRS): a potential method for the detection of neuronal currents with MRI. Neuroimage. 2008; 42:1357–65. [PubMed: 18684643]

27. Jiang X, Sheng J, Li H, Chai Y, Zhou X, Wu B, Guo X, Gao J-H. Detection of subnanotesla oscillatory magnetic fields using MRI. Magn Reson Med. 2016; 75:519–526. [PubMed: 25753110]

28. Luo Q, Lu H, Lu H, Senseman D, Worsley K, Yang Y, Gao J-H. Physiologically evoked neuronal current MRI in a bloodless turtle brain: Detectable or not? Neuroimage. 2009; 47:1268–1276. [PubMed: 19539040]

29. Sundaram P, Nummenmaa A, Wells W, Orbach D, Orringer D, Mulkern R, Okada Y. Direct neural current imaging in an intact cerebellum with magnetic resonance imaging. Neuroimage. 2016; 132:477–490. [PubMed: 26899788]

30. Pohmann R, Speck O, Scheffler K. Signal-to-noise ratio and MR tissue parameters in human brain imaging at 3, 7, and 9.4 tesla using current receive coil arrays. Magn Reson Med. 2016; 75:801–9. [PubMed: 25820458]

31. Uludağ K, Müller-Bierl B, Uğurbil K. An integrative model for neuronal activity-induced signal changes for gradient and spin echo functional imaging. Neuroimage. 2009; 48:150–65. [PubMed: 19481163]

32. Setsompop K, Feinberg DA, Polimeni JR. Rapid brain MRI acquisition techniques at ultra-high fields. NMR Biomed. 2016; 29:1198–221. [PubMed: 26835884]

33•. Budinger TF, Bird MD, Frydman L, Long JR, Mareci TH, Rooney WD, Rosen B, Schenck JF, Schepkin VD, Sherry AD, et al. Toward 20 T magnetic resonance for human brain studies: opportunities for discovery and neuroscience rationale. Magn Reson Mater Physics, Biol Med. 2016; 29:617–639. This review lays out arguments for the benefits of pushing human MRI beyond the current maximal field strengths of 9.4 Tesla–11.7 Tesla. The many technical challenges are outlined, and—based on the engineering efforts made to develop the current generation of UHF scanners—the solutions to these challenges may already be at hand.

34. Le Bihan D, Schild T. Human brain MRI at 500 MHz, scientific perspectives and technological challenges. Supercond Sci Technol. 2017; 30:33003.

35•. Eryaman Y, Zhang P, Utecht L, Kose K, Lagore RL, DelaBarre L, Kulesa J, Eberly LE, Adriany G, Iles TL, et al. Investigating the physiological effects of 10.5 Tesla static field exposure on anesthetized swine. Magn Reson Med. 2018; 79:511–514. This study presents the initial experimental data on the safety of a recently constructed whole-body human MRI scanner at 10.5 Tesla. [PubMed: 28342176]

36. Keil B, Wald LL. Massively parallel MRI detector arrays. J Magn Reson. 2013; 229:75–89. [PubMed: 23453758]

37. Preibisch C, Pilatus U, Bunke J, Hoogenraad F, Zanella F, Lanfermann H. Functional MRI using sensitivity-encoded echo planar imaging (SENSE-EPI). Neuroimage. 2003; 19:412–421. [PubMed: 12814590]

38. de Zwart JA, van Gelderen P, Kellman P, Duyn JH. Application of sensitivity-encoded echo-planar imaging for blood oxygen level-dependent functional brain imaging. Magn Reson Med. 2002; 48:1011–20. [PubMed: 12465111]

39. Weiger M, Pruessmann KP, Osterbauer R, Börnert P, Boesiger P, Jezzard P. Sensitivity-encoded single-shot spiral imaging for reduced susceptibility artifacts in BOLD fMRI. Magn Reson Med. 2002; 48:860–6. [PubMed: 12418001]

40. Keil B, Blau JN, Biber S, Hoecht P, Tountcheva V, Setsompop K, Triantafyllou C, Wald LL. A 64-channel 3T array coil for accelerated brain MRI. Magn Reson Med. 2013; 70:248–58. [PubMed: 22851312]

41. Wiggins GC, Polimeni JR, Potthast A, Schmitt M, Alagappan V, Wald LL. 96-Channel receive-only head coil for 3 Tesla: design optimization and evaluation. Magn Reson Med. 2009; 62:754–62. [PubMed: 19623621]

42. Auerbach E, DelaBarre L, Van de Moortele P-F, Strupp J, Gumbrecht R, Potthast A, Pirkl G, Moeller S, Hanna B, Grant A, et al. An integrated 32-channel transmit and 64-channel receive 7 tesla MRI system. Proc Intl Soc Mag Reson Med. 2017; 25:1218.

43. Farivar R, Grigorov F, van der Kouwe AJW, Wald LL, Keil B. Dense, shape-optimized posterior 32-channel coil for submillimeter functional imaging of visual cortex at 3T. Magn Reson Med. 2016; 76:321–8. [PubMed: 26218835]

44. Keil B, Sappo C, Bilgic B, Polimeni JR, Golestani L, Etzel R, Wald LL, Feinberg DA, Setsompop K. Sub-millimeter cortical imaging at 7T using a high-density motor-cortex 32-channel array coil. Proc Intl Soc Mag Reson Med. 2017; 25:1224.

45•. Petridou N, Italiaander M, van de Bank BL, Siero JCW, Luijten PR, Klomp DWJ. Pushing the limits of high-resolution functional MRI using a simple high-density multi-element coil design. NMR Biomed. 2013; 26:65–73. This article demonstrated the feasibility and performance of a high-density RF receive coil array consisting of 32 small elements surrounding only the occipital cortex to maximize sensitivity and parallel imaging performance within this region. The success of this design suggests that similar high-density arrays can be extended across the entire brain. [PubMed: 22674638]

46. Pruessmann KP, Weiger M, Scheidegger MB, Boesiger P. SENSE: sensitivity encoding for fast MRI. Magn Reson Med. 1999; 42:952–62. [PubMed: 10542355]

47. Griswold MA, Jakob PM, Heidemann RM, Nittka M, Jellus V, Wang J, Kiefer B, Haase A. Generalized autocalibrating partially parallel acquisitions (GRAPPA). Magn Reson Med. 2002; 47:1202–10. [PubMed: 12111967]

48. Breuer FA, Blaimer M, Heidemann RM, Mueller MF, Griswold MA, Jakob PM. Controlled aliasing in parallel imaging results in higher acceleration (CAIPIRINHA) for multi-slice imaging. Magn Reson Med. 2005; 53:684–91. [PubMed: 15723404]

49••. Breuer FA, Blaimer M, Mueller MF, Seiberlich N, Heidemann RM, Griswold MA, Jakob PM. Controlled aliasing in volumetric parallel imaging (2D CAIPIRINHA). Magn Reson Med. 2006; 55:549–556. In this follow-up to this group's 2005 article, the concept of Controlled Aliasing was fully developed and extended into a general framework in which the sampling pattern of the k-space data could be designed to yield a more favorable aliasing pattern and therefore a more effective image reconstruction. [PubMed: 16408271]

50. Ye H, Cauley SF, Gagoski B, Bilgic B, Ma D, Jiang Y, Du YP, Griswold MA, Wald LL, Setsompop K. Simultaneous multislice magnetic resonance fingerprinting (SMS-MRF) with direct-spiral slice-GRAPPA (ds-SG) reconstruction. Magn Reson Med. 2017; 77:1966–1974. [PubMed: 27220881]

51. Bilgic B, Goyal VK, Adalsteinsson E. Multi-contrast reconstruction with Bayesian compressed sensing. Magn Reson Med. 2011; 66:1601–1615. [PubMed: 21671267]

52. Breuer FA, Moriguchi H, Seiberlich N, Blaimer M, Jakob PM, Duerk JL, Griswold MA. Zigzag sampling for improved parallel imaging. Magn Reson Med. 2008; 60:474–8. [PubMed: 18666134]

53. Moriguchi H, Duerk JL. Bunched phase encoding (BPE): a new fast data acquisition method in MRI. Magn Reson Med. 2006; 55:633–48. [PubMed: 16470597]

54•. Bilgic B, Gagoski BA, Cauley SF, Fan AP, Polimeni JR, Grant PE, Wald LL, Setsompop K. Wave-CAIPI for highly accelerated 3D imaging. Magn Reson Med. 2015; 73:2152–2162. The wave-CAIPI technique introduced in this article extended the concept of Controlled Aliasing into all three encoding dimensions through the use of a corkscrew ("wave") readout trajectory, providing dramatic improvements in artifact level and signal-to-noise ratio in volumetric anatomical imaging compared to conventional parallel imaging acceleration approaches. [PubMed: 24986223]

55. Gagoski BA, Bilgic B, Eichner C, Bhat H, Grant PE, Wald LL, Setsompop K. RARE/turbo spin echo imaging with Simultaneous Multislice Wave-CAIPI. Magn Reson Med. 2015; 73:929–938. [PubMed: 25640187]

56. Cauley SF, Setsompop K, Bilgic B, Bhat H, Gagoski B, Wald LL. Autocalibrated wave-CAIPI reconstruction; Joint optimization of k-space trajectory and parallel imaging reconstruction. Magn Reson Med. 2017; 78:1093–1099. [PubMed: 27770457]

57. Polak D, Setsompop K, Cauley SF, Gagoski BA, Bhat H, Maier F, Bachert P, Wald LL, Bilgic B. Wave-CAIPI for highly accelerated MP-RAGE imaging. Magn Reson Med. 2018; 79:401–406. [PubMed: 28220617]

58. Bilgic B, Xie L, Dibb R, Langkammer C, Mutluay A, Ye H, Polimeni JR, Augustinack J, Liu C, Wald LL, et al. Rapid multi-orientation quantitative susceptibility mapping. Neuroimage. 2016; 125:1131–1141. [PubMed: 26277773]

59. Larkman DJ, Hajnal JV, Herlihy AH, Coutts GA, Young IR, Ehnholm G. Use of multicoil arrays for separation of signal from multiple slices simultaneously excited. J Magn Reson Imaging. 2001; 13:313–7. [PubMed: 11169840]

60. Nunes RG, Hajnal JV, Golay X, Larkman DJ. Simultaneous slice excitation and reconstruction for single shot EPI. Proc Intl Soc Mag Reson Med. 2006; 14:293.

61•. Barth M, Breuer FA, Koopmans PJ, Norris DG, Poser BA. Simultaneous multislice (SMS) imaging techniques. Magn Reson Med. 2015; 75:63–81. This review article describes a successful scheme for applying Controlled Aliasing (CAIPI) to Simultaneous Multi-Slice (SMS) Echo-Planar Imaging (EPI). The “blipped CAIPI” method uses self-refocusing slice-select gradient blips to apply the CAIPI shift between slices, providing far higher acceleration capabilities than what could be achieved without the use of Controlled Aliasing. This blipped-CAIPI technique is the basis of all modern Simultaneous Multi-Slice EPI that is used in functional, diffusion, and perfusion imaging. [PubMed: 26308571]

62. Setsompop K, Gagoski BA, Polimeni JR, Witzel T, Wedeen VJ, Wald LL. Blipped-controlled aliasing in parallel imaging for simultaneous multislice echo planar imaging with reduced g-factor penalty. Magn Reson Med. 2012; 67:1210–24. [PubMed: 21858868]

63. Feinberg DA, Moeller S, Smith SM, Auerbach E, Ramanna S, Glasser MF, Miller KL, Uğurbil K, Yacoub E. Multiplexed Echo Planar Imaging for sub-second whole brain fMRI and fast diffusion imaging. PLoS One. 2010; 5:e15710. [PubMed: 21187930]

64. Moeller S, Yacoub E, Olman CA, Auerbach E, Strupp J, Harel N, Uğurbil K. Multiband multislice GE-EPI at 7 Tesla, with 16-fold acceleration using partial parallel imaging with application to high spatial and temporal whole-brain fMRI. Magn Reson Med. 2010; 63:1144–53. [PubMed: 20432285]

65. Feinberg DA, Setsompop K. Ultra-fast MRI of the human brain with simultaneous multi-slice imaging. J Magn Reson. 2013; 229:90–100. [PubMed: 23473893]

66. Lustig M, Donoho D, Pauly JM. Sparse MRI: The application of compressed sensing for rapid MR imaging. Magn Reson Med. 2007; 58:1182–95. [PubMed: 17969013]

67. Ma D, Gulani V, Seiberlich N, Liu K, Sunshine JL, Duerk JL, Griswold MA. Magnetic resonance fingerprinting. Nature. 2013; 495:187–92. [PubMed: 23486058]

68. Gong E, Zaharchuk G, Pauly J. Improving the PI+CS Reconstruction for Highly Undersampled Multi-contrast MRI using Local Deep Network. Proc Intl Soc Mag Reson Med. 2017; 25:5663.

69•. Zhu B, Liu JZ, Cauley SF, Rosen BR, Rosen MS. Image reconstruction by domain-transform manifold learning. Nature. 2018; 555:487–492. This study demonstrates the potential for machine learning techniques to aid in MR image reconstruction. After training a neural network only on a set of natural images, the authors demonstrate that the network could generalize to reconstruct clinical MR images and, remarkably, can outperform modern parallel imaging methods when applied to undersampled data. [PubMed: 29565357]

70. Eo T, Jun Y, Kim T, Jang J, Lee H-J, Hwang D. KIKI-net: cross-domain convolutional neural networks for reconstructing undersampled magnetic resonance images. Magn Reson Med. 2018; doi: 10.1002/mrm.27201

71. Schlemper J, Caballero J, Hajnal JV, Price AN, Rueckert D. A deep cascade of Convolutional Neural Networks for dynamic MR image reconstruction. IEEE Trans Med Imaging. 2018; 37:491–503. [PubMed: 29035212]

72. Heidemann RM, Ivanov D, Trampel R, Fasano F, Meyer H, Pfeuffer J, Turner R. Isotropic submillimeter fMRI in the human brain at 7 T: combining reduced field-of-view imaging and partially parallel acquisitions. Magn Reson Med. 2012; 68:1506–16. [PubMed: 22231859]

73. Feinberg DA, Harel N, Ramanna S, Uğurbil K, Yacoub E. Sub-millimeter single-shot 3D GRASE with inner volume selection for T2-weighted fMRI applications at 7 Tesla. Proc Intl Soc Mag Reson Med. 2008; 16:2373.

74. Schneider R, Ritter D, Haueisen J, Pfeuffer J. B0-informed variable density trajectory design for enhanced correction of off-resonance effects in parallel transmission. Magn Reson Med. 2014; 71:1381–1393. [PubMed: 23716347]

75. Waggoner RA, Ueno K, Pfeuffer J, Tanaka K, Cheng K. High-Resolution fMRI of the visual system at 3T using Zoomed Excitation via Tx-SENSE. Proc Intl Soc Mag Reson Med. 2017; 25:5227.

76. Setsompop K, Alagappan V, Gagoski B, Witzel T, Polimeni JR, Potthast A, Hebrank F, Fontius U, Schmitt F, Wald LL, et al. Slice-selective RF pulses for in vivo B1+ inhomogeneity mitigation at 7 tesla using parallel RF excitation with a 16-element coil. Magn Reson Med. 2008; 60:1422–32. [PubMed: 19025908]

77. Guérin B, Gebhardt M, Cauley S, Adalsteinsson E, Wald LL. Local specific absorption rate (SAR), global SAR, transmitter power, and excitation accuracy trade-offs in low flip-angle parallel transmit pulse design. Magn Reson Med. 2014; 71:1446–57. [PubMed: 23776100]

78. Brunner DO, Pruessmann KP. Optimal design of multiple-channel RF pulses under strict power and SAR constraints. Magn Reson Med. 2010; 63:1280–1291. [PubMed: 20432299]

79. Juchem C, Nixon TW, McIntyre S, Boer VO, Rothman DL, de Graaf RA. Dynamic multi-coil shimming of the human brain at 7 T. J Magn Reson. 2011; 212:280–8. [PubMed: 21824794]

80. Pan JW, Lo K-M, Hetherington HP. Role of very high order and degree B0 shimming for spectroscopic imaging of the human brain at 7 tesla. Magn Reson Med. 2012; 68:1007–17. [PubMed: 22213108]

81•. Stockmann JP, Witzel T, Keil B, Polimeni JR, Mareyam A, LaPierre C, Setsompop K, Wald LL. A 32-channel combined RF and B0 shim array for 3T brain imaging. Magn Reson Med. 2016; 75:441–51. This study demonstrated the “AC/DC” concept of combining B_0 shimming elements (“DC”) with the RF detector coils (“AC”) on a single conductor. The resulting 32-channel B_0 shim array provided additional degrees of freedom to compensate for high-spatial-order B_0 nonuniformities in the head, and is capable of rapid field control for dynamic, real-time corrections. [PubMed: 25689977]

82. Truong T-K, Darnell D, Song AW. Integrated RF/shim coil array for parallel reception and localized B0 shimming in the human brain. Neuroimage. 2014; 103:235–40. [PubMed: 25270602]

83. Stockmann JP, Wald LL. In vivo B0 field shimming methods for MRI at 7T. Neuroimage. 2017; doi: 10.1016/j.neuroimage.2017.06.013

84. De Zanche N, Barmet C, Nordmeyer-Massner JA, Pruessmann KP. NMR probes for measuring magnetic fields and field dynamics in MR systems. Magn Reson Med. 2008; 60:176–86. [PubMed: 18581363]

85. Duerst Y, Wilm BJ, Dietrich BE, Vannesjo SJ, Barmet C, Schmid T, Brunner DO, Pruessmann KP. Real-time feedback for spatiotemporal field stabilization in MR systems. Magn Reson Med. 2015; 73:884–93. [PubMed: 24634192]

86. Tountcheva V, Keil B, Witzel T, Tisdall D, Hoecht P, Wald LL. A 64 channel receive-only field camera for eddy current and trajectory calibration. Proc Intl Soc Mag Reson Med. 2012; 20:701.

87. Chu Y-H, Hsu Y-C, Lin F-H. Decoupled dynamic magnetic field measurements improves diffusion-weighted magnetic resonance images. Sci Rep. 2017; 7:11630. [PubMed: 28912538]

88. Giese D, Haeberlin M, Barmet C, Pruessmann KP, Schaeffter T, Kozerke S. Analysis and correction of background velocity offsets in phase-contrast flow measurements using magnetic field monitoring. Magn Reson Med. 2012; 67:1294–302. [PubMed: 21826731]

89•. Kasper L, Engel M, Barmet C, Haeberlin M, Wilm BJ, Dietrich BE, Schmid T, Gross S, Brunner DO, Stephan KE, et al. Rapid anatomical brain imaging using spiral acquisition and an expanded signal model. Neuroimage. 2018; This article demonstrated the use of magnetic field monitoring for the correction of both static and dynamic magnetic field offsets during human fMRI scanning, and utilized these measurements to reconstruct 2D spiral images with extraordinary image quality. doi: 10.1016/j.neuroimage.2017.07.062

90. Vannesjo SJ, Wilm BJ, Duerst Y, Gross S, Brunner DO, Dietrich BE, Schmid T, Barmet C, Pruessmann KP. Retrospective correction of physiological field fluctuations in high-field brain MRI using concurrent field monitoring. Magn Reson Med. 2015; 73:1833–43. [PubMed: 24903278]

91. Gross S, Vionnet L, Kasper L, Dietrich BE, Pruessmann KP. Physiology recording with magnetic field probes for fMRI denoising. Neuroimage. 2017; 154:106–114. [PubMed: 28088483]

92. Turner R. Gradient coil design: a review of methods. Magn Reson Imaging. 1993; 11:903–920. [PubMed: 8231676]

93•. Tan ET, Lee S-K, Weavers PT, Graziani D, Piel JE, Shu Y, Huston J, Bernstein MA, Foo TKF. High slew-rate head-only gradient for improving distortion in echo planar imaging: Preliminary experience. J Magn Reson Imaging. 2016; 44:653–64. This study demonstrates the ability of high slew-rate head gradient coils to avoid Peripheral Nerve Stimulation—because the gradient fields only extend over the head and neck, head gradients avoid stimulation in the torso and shoulders during high-slewrate readouts. The advantages of high slew-rate for echo-planar imaging quality including distortion and blurring is demonstrated. [PubMed: 26921117]

94. Lee S-K, Mathieu J-B, Graziani D, Piel J, Budesheim E, Fiveland E, Hardy CJ, Tan ET, Amm B, Foo TK-F, et al. Peripheral nerve stimulation characteristics of an asymmetric head-only gradient coil compatible with a high-channel-count receiver array. Magn Reson Med. 2016; 76:1939–1950. [PubMed: 26628078]

95. Winkler SA, Alejski A, Wade T, McKenzie CA, Rutt BK. On the accurate analysis of vibroacoustics in head insert gradient coils. Magn Reson Med. 2017; 78:1635–1645. [PubMed: 27859549]

96•. Davids M, Guérin B, Malzacher M, Schad LR, Wald LL. Predicting magnetostimulation thresholds in the Peripheral Nervous System using realistic body models. Sci Rep. 2017; 7:5316. This article introduces a numerical simulation framework based on a full-body nerve anatomy and nerve dynamics model to predict the threshold and location for which a given gradient coil winding pattern initiates Peripheral Nerve Stimulation in humans. [PubMed: 28706244]

97. Kroboth S, Layton KJ, Jia F, Littin S, Yu H, Hennig J, Zaitsev M. Optimization of coil element configurations for a matrix gradient coil. IEEE Trans Med Imaging. 2018; doi: 10.1109/TMI.2017.2743463

98. Littin S, Jia F, Layton KJ, Kroboth S, Yu H, Hennig J, Zaitsev M. Development and implementation of an 84-channel matrix gradient coil. Magn Reson Med. 2018; doi: 10.1002/mrm.26700

99. Gallichan D, Cocosco CA, Schultz G, Weber H, Welz AM, Hennig J, Zaitsev M. Practical considerations for in vivo MRI with higher dimensional spatial encoding. Magn Reson Mater Physics, Biol Med. 2012; 25:419–31.

100. Lin F-H. Multidimensionally encoded magnetic resonance imaging. Magn Reson Med. 2013; 70:86–96. [PubMed: 22926830]

101. Hennig J, Welz AM, Schultz G, Korvink J, Liu Z, Speck O, Zaitsev M. Parallel imaging in non-bijective, curvilinear magnetic field gradients: a concept study. Magn Reson Mater Physics, Biol Med. 2008; 21:5–14.

102. Stockmann JP, Ciris PA, Galiana G, Tam L, Constable RT. O-space imaging: Highly efficient parallel imaging using second-order nonlinear fields as encoding gradients with no phase encoding. Magn Reson Med. 2010; 64:447–56. [PubMed: 20665789]

103. Setsompop K, Kimmlingen R, Eberlein E, Witzel T, Cohen-Adad J, McNab JA, Keil B, Tisdall MD, Hoecht P, Dietz P, et al. Pushing the limits of in vivo diffusion MRI for the Human Connectome Project. Neuroimage. 2013; 80:220–33. [PubMed: 23707579]

104. McNab JA, Edlow BL, Witzel T, Huang SY, Bhat H, Heberlein K, Feiweier T, Liu K, Keil B, Cohen-Adad J, et al. The Human Connectome Project and beyond: initial applications of 300 mT/m gradients. Neuroimage. 2013; 80:234–45. [PubMed: 23711537]

105. Ferizi U, Scherrer B, Schneider T, Alipoor M, Eufracio O, Fick RHJ, Deriche R, Nilsson M, Loya-Olivas AK, Rivera M, et al. Diffusion MRI microstructure models with in vivo human brain Connectome data: results from a multi-group comparison. NMR Biomed. 2017; 30:e3734.

106. Huang SY, Nummenmaa A, Witzel T, Duval T, Cohen-Adad J, Wald LL, McNab JA. The impact of gradient strength on in vivo diffusion MRI estimates of axon diameter. Neuroimage. 2015; 106:464–72. [PubMed: 25498429]

107. Uğurbil K, Xu J, Auerbach EJ, Moeller S, Vu AT, Duarte-Carvajalino JM, Lenglet C, Wu X, Schmitter S, Van de Moortele P-F, et al. Pushing spatial and temporal resolution for functional and diffusion MRI in the Human Connectome Project. Neuroimage. 2013; 80:80–104. [PubMed: 23702417]

108•. Sander CY, Keil B, Chonde DB, Rosen BR, Catana C, Wald LL. A 31-channel MR brain array coil compatible with positron emission tomography. Magn Reson Med. 2015; 73:2363–75. This study combines a MR-compatible PET camera head insert, for high-resolution PET imaging, with a custom MR RF array coil detector designed to minimally influence concurrent PET detection. This instrumentation was subsequently applied to acquire simultaneous dynamic PET/fMRI data. [PubMed: 25046699]

109. Shah NJ, Oros-Peusquens A-M, Arrubla J, Zhang K, Warbrick T, Mauler J, Vahedipour K, Romanzetti S, Felder J, Celik A, et al. Advances in multimodal neuroimaging: hybrid MR-PET and MR-PET-EEG at 3 T and 94 T. J Magn Reson. 2013; 229:101–15. [PubMed: 23317760]

110. Pichler BJ, Judenhofer MS, Catana C, Walton JH, Kneilling M, Nutt RE, Siegel SB, Claussen CD, Cherry SR. Performance test of an LSO-APD detector in a 7-T MRI scanner for simultaneous PET/MRI. J Nucl Med. 2006; 47:639–47. [PubMed: 16595498]

111. Wey H-Y, Catana C, Hooker JM, Dougherty DD, Knudsen GM, Wang DJJ, Chonde DB, Rosen BR, Gollub RL, Kong J. Simultaneous fMRI-PET of the opioidergic pain system in human brain. Neuroimage. 2014; 102(Pt 2):275–82. [PubMed: 25107855]

112. Sander CY, Hooker JM, Catana C, Normandin MD, Alpert NM, Knudsen GM, Vanduffel W, Rosen BR, Mandeville JB. Neurovascular coupling to D2/D3 dopamine receptor occupancy using simultaneous PET/functional MRI. Proc Natl Acad Sci U S A. 2013; 110:11169–74. [PubMed: 23723346]

113. Mullinger K, Brookes M, Stevenson C, Morgan P, Bowtell R. Exploring the feasibility of simultaneous electroencephalography/functional magnetic resonance imaging at 7 T. Magn Reson Imaging. 2008; 26:968–77. [PubMed: 18508217]

114. Vasios CE, Angelone LM, Purdon PL, Ahveninen J, Belliveau JW, Bonmassar G. EEG/(f)MRI measurements at 7 Tesla using a new EEG cap ("InkCap"). Neuroimage. 2006; 33:1082–92. [PubMed: 17035045]

115. Jorge J, Grouiller F, Ipek Ö, Stoermer R, Michel CM, Figueiredo P, van der Zwaag W, Gruetter R. Simultaneous EEG-fMRI at ultra-high field: artifact prevention and safety assessment. Neuroimage. 2015; 105:132–44. [PubMed: 25449743]

116. Lewis, L., Polimeni, JR., Setsompop, K., Witzel, T., Rosen, BR., Bonmassar, G. Detecting thalamic correlates of cortical oscillations using simultaneous EEG-fMRI at 7 Tesla. 23rd Annu Meet Organ Hum Brain Mapping; June 25–29, 2017; Vancouver, BC, Canada. 2017. p. 23

117. Navarro de Lara LI, Tik M, Woletz M, Frass-Kriegl R, Moser E, Laistler E, Windischberger C. High-sensitivity TMS/fMRI of the human motor cortex using a dedicated multichannel MR coil. Neuroimage. 2017; 150:262–269. [PubMed: 28254457]

118. Ruff CC, Driver J, Bestmann S. Combining TMS and fMRI: from "virtual lesions" to functional-network accounts of cognition. Cortex. 2009; 45:1043–9. [PubMed: 19166996]

119. Bystritsky A, Korb AS, Douglas PK, Cohen MS, Melega WP, Mulgaonkar AP, DeSalles A, Min B-K, Yoo S-S. A review of low-intensity focused ultrasound pulsation. Brain Stimul. 2011; 4:125–136. [PubMed: 21777872]

120. Lee W, Kim H-C, Jung Y, Chung YA, Song I-U, Lee J-H, Yoo S-S. Transcranial focused ultrasound stimulation of human primary visual cortex. Sci Rep. 2016; 6:34026. [PubMed: 27658372]

121. Legon W, Sato TF, Opitz A, Mueller J, Barbour A, Williams A, Tyler WJ. Transcranial focused ultrasound modulates the activity of primary somatosensory cortex in humans. Nat Neurosci. 2014; 17:322–329. [PubMed: 24413698]

122. Sato T, Shapiro M, Tsao D. Ultrasonic neuromodulation causes widespread cortical activation via an indirect auditory mechanism. bioRxiv. 2017; doi: 10.1101/234211

123. Guo H, Hamilton M, Offutt SJ, Gloeckner CD, Li T, Kim Y, Legon W, Alford JK, Lim HH. Ultrasound produces extensive brain activation via a cochlear pathway. bioRxiv. 2017; doi: 10.1101/233189

HIGHLIGHTS

- Spatial scale of hemodynamic response is finer than fMRI resolution achievable today
- Improving fMRI resolution requires increases in sensitivity and image encoding
- Sensitivity can be increased with higher magnetic fields and dense detector arrays
- Image encoding can be sped up with fast gradient coils & efficient sampling schemes
- These advances will narrow the gap between noninvasive fMRI and optical imaging

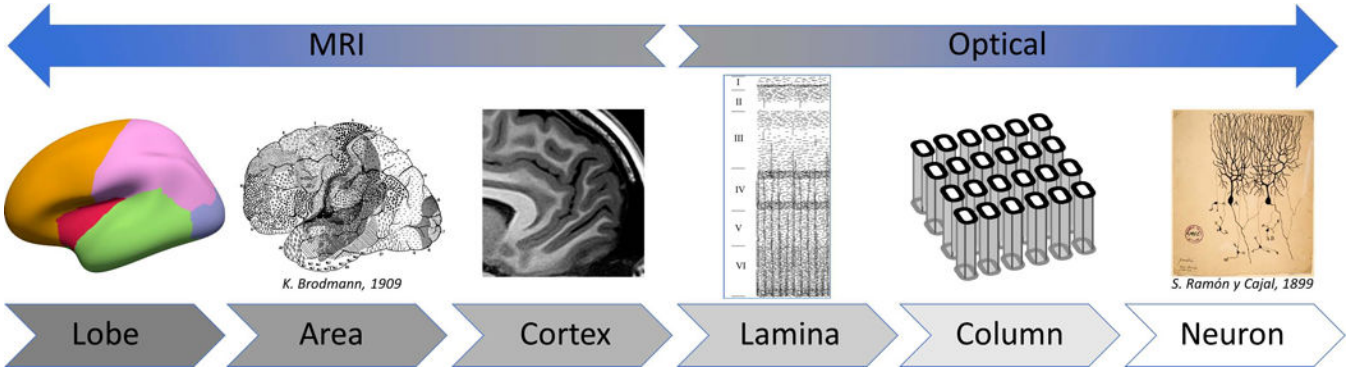

Fig. 1. Scales of functional architecture accessible to fMRI in humans and to optical imaging in animal models

Although continued technological development has decreased the spatial resolution of human fMRI to the submillimeter scale, further developments will be required to resolve units of cortical functional architecture such as cortical columns and layers over the entire brain. At the same time, invasive optical imaging techniques have expanded their spatial coverage to several millimeters, and in some cases an image plane covering a slice of the entire two cerebral hemispheres. Recent studies have shown that as these two complementary imaging modalities converge they can inform one another, yielding new insights into brain function. Further technological advances are required to continue to enhance the spatial resolution and neuronal specificity of human fMRI while retaining whole-brain coverage.

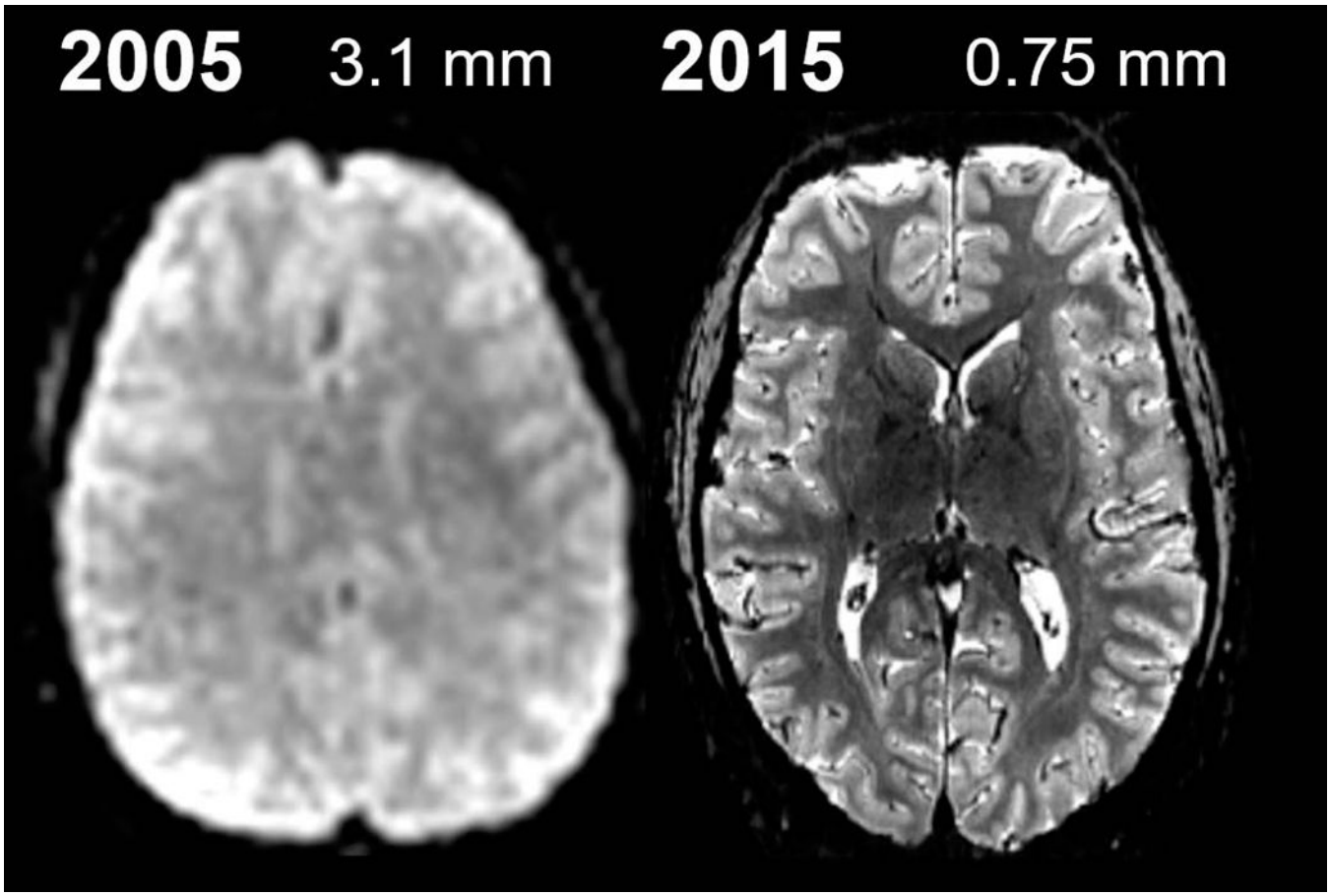

Fig. 2. Recent progress in fMRI spatial resolution and image quality

(**Left**) A standard 3 Tesla 3.1 mm isotropic echo-planar image used for conventional fMRI studies circa 2005. (**Right**) A more recent example of 7 Tesla 0.75 mm isotropic echo-planar image, acquired with parallel imaging acceleration and a 32-channel RF coil array and a specialized head gradient coil to achieve a four-fold accelerated rapid readout. Continued technology development will be needed to surpass this resolution for whole-brain neuroimaging studies.

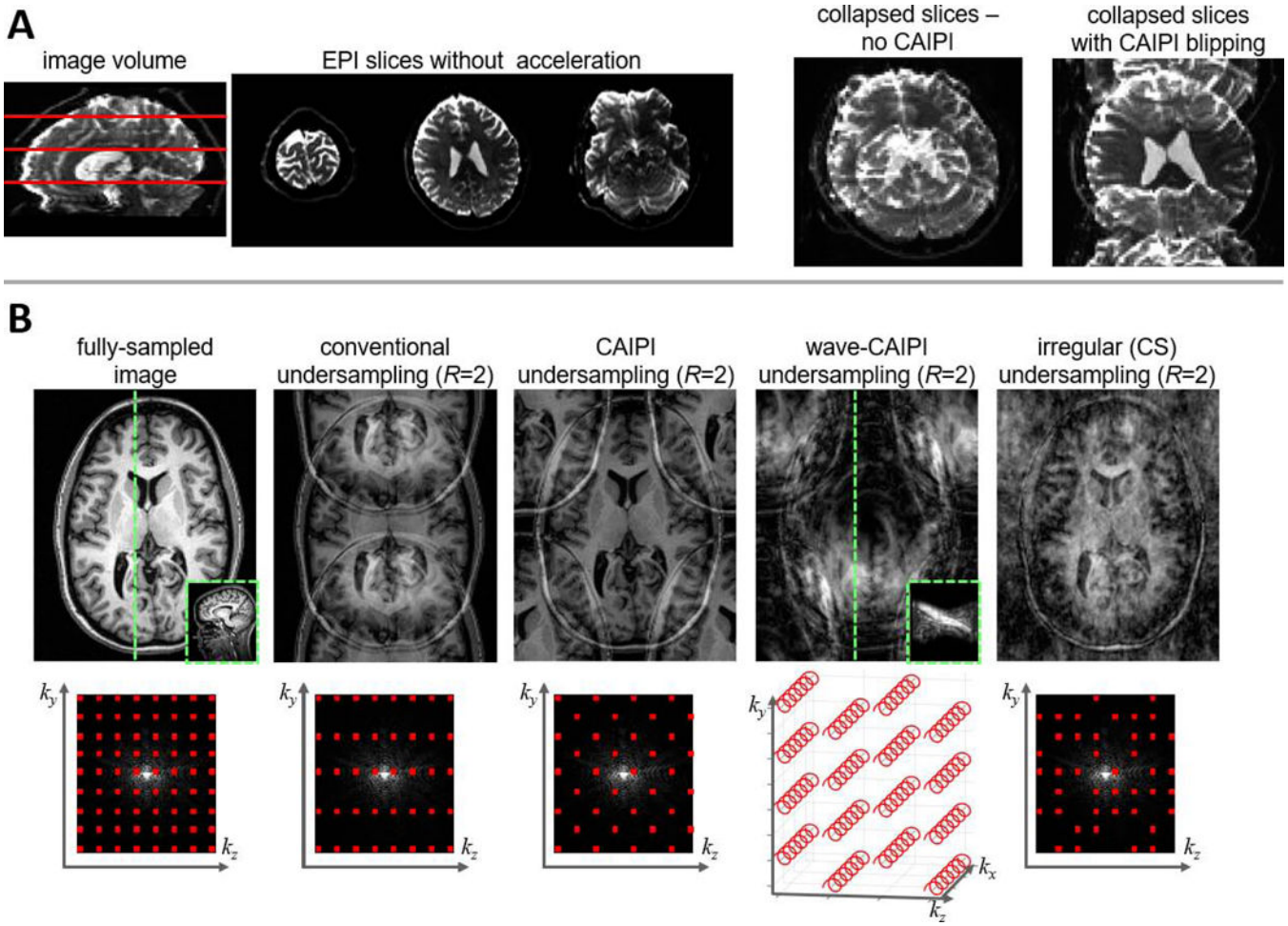

Fig. 3. Sampling schemes used for efficient image encoding in accelerated MRI

The time taken to encode an image can be reduced by skipping samples in Fourier or k-space, and the aliasing artifacts induced by this undersampling can be removed during image reconstruction through parallel imaging techniques. This allows one to accelerate the acquisition and still (ideally) produce an alias-free image. The distribution of aliasing in the image however is determined by the sampling pattern in k-space, and some patterns of aliasing are more amenable to removal via parallel imaging reconstruction than others. (**A**) Example of the application of CAIPI to Simultaneous Multi-Slice EPI. In this example, three axial slices are acquired simultaneously; the locations of the three example slices are shown in red in the sagittal reformat of the data. During acquisition, “blipping” the z-gradient imposes a slice-specific shift such that the acquired, collapsed images exhibit less overlap compared to the case without CAIPI shifting. (Adapted from Ref. [62], with permission.) Acquiring multiple EPI slices simultaneously increases the image encoding efficiency and therefore increases temporal resolution. (**B**) Illustration of undersampling schemes applicable to 2D or 3D imaging. Shown are images directly reconstructed from the undersampled data to demonstrate the pattern of aliasing that must be removed in each case (top row). Simplified schematics of the corresponding undersampling patterns in k-space are provided (bottom row). In each case an undersampling factor of 2 is applied to 3D encoded

data. In the case of CAIPI undersampling, the data are still undersampled by a factor of 2 but the samples are shifted into a “quincunx” pattern to cause aliased replicates to fall into the corners of the image. In the case of wave-CAIPI, the same “quincunx” undersampling is performed combined with “wave” readouts to spread aliasing into the readout direction (head-to-foot) as well; to demonstrate this effect, the insets shown in the original image (for reference) and in the wave-CAIPI image show a sagittal slice through the volume at the location of the dashed green line. In the irregular Compressed Sensing undersampling, the sampling pattern is pseudo-random but still achieves an overall undersampling factor of 2; in this case the aliasing appears incoherent or noise-like in the direct reconstruction.